RESEARCH ARTICLE

JOURNAL OF Applied Polymer SCIENCE WILEY

E/Z reversible photoisomerization of methyl orange doped polyacrylic acid-based polyelectrolyte brush films

Qais M. Al-Bataineh[1,2,3] | Ahmad D. Telfah[1,4] | Ahmad A. Ahmad[3] |
Areen A. Bani-Salameh[3] | Rund Abu-Zurayk[4,5] | Roland Hergenröder[1]

[1]Leibniz Institut für Analytische Wissenschaften-ISAS-e.V., Dortmund, Germany

[2]Experimental Physics, TU Dortmund University, Dortmund, Germany

[3]Department of Physics, Jordan University of Science & Technology, Irbid, Jordan

[4]Nanotechnology Center, The University of Jordan, Amman, Jordan

[5]Hamdi Mango Center for Scientific Research, The University of Jordan, Amman, Jordan

Correspondence
Ahmad D. Telfah, Leibniz Institut für Analytische Wissenschaften-ISAS-e.V., Bunsen-Kirchhoff-Straße 11, 44139 Dortmund, Germany.
Email: telfah.ahmad@isas.de

Abstract

The photoswitching behavior of the polyacrylic acid (PAA) doped by methyl orange (MO) brush film was investigated using spectral analysis of UV-Vis absorbance, Fourier Transformation Infrared spectroscopy, 2D electrical conductivity mapping and Atomic Force Microscopy. The kinetics and time evolution of the photoisomerization of the PAA-MO PEBs film from E-state to Z-state by UV-light irradiation, and reverse thermal relaxation to E-state was explored. The results confirm that the photoisomerization kinetics of the overall peak is the superposition of the photoisomerization kinetics of $S_2(\pi\pi^*)$ transition, low- and high-frequency of the $S_1(n\pi^*)$ transition bands. The E–Z transformation led to transforming the azobenzene from flat with no dipole moment to 3.0 D dipole moment. Hence, the electrical conductivity escalated accordingly. The transformation of E-state to Z-state led to the collapse of the formed brushes because of the angular rotational momentum consequent to E–Z isomerization.

KEYWORDS

E–Z isomerization, methyl orange (MO), photoisomerization, polyacrylic acid (PAA), polyelectrolytes

1 | INTRODUCTION

Polyelectrolytes brushes (PEBs) are charged polymers deposited as a brush-like structure on a substrate used in many applications, such as intelligent actuators, protein refinement, drug delivery, and bioelectronic devices.[1–4] Many parameters affect the swelling behavior of PEBs, such as temperature,[5] electric field,[6] pH,[7] or photoirradiation frequency.[8] Polyacrylic acid (PAA) is an active PEBs

that changes its structures, charges, and hydrophilicity due to electrostatic properties. PAA PEBs induce the polymer chains' conformational stretching by electrostatic repulsion of the negatively charged COO^- groups, and consequently, converting the hydrophobic behavior of the PAA PEBs into hydrophilic behavior.[9]

Photoswitch molecules are transformed from one geometric form to another by exposing their molecules to light. Azobenzene and its derivatives are the main
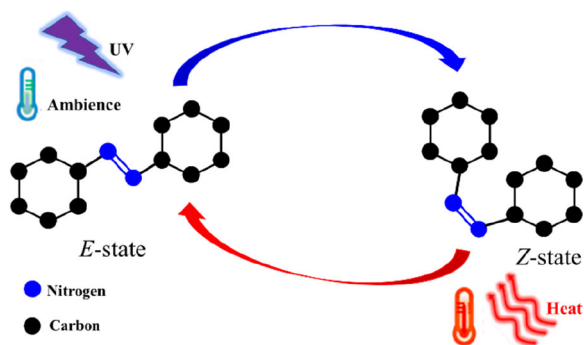
FIGURE 1 Schematic diagram of the photoisomerization process of azobenzene. [Color figure can be viewed at wileyonlinelibrary.com]

photoswitch molecules composed of organic molecules in the ring shapes connected by the conjugated azo group (—N=N—). Azobenzene derivatives are used in many applications, such as intelligent actuators, photochromic molecular switches, molecular solar thermal energy storage media, and targeted activation or release of drugs.[10–16] In addition, azobenzene and its derivatives can change the chemical group connecting with the aromatic rings to get a new geometry, which leads to changing the donation/withdrawing for electron distribution.[17,18] For most azobenzene derivatives, the initial state is the E-state since it is more stable than the Z-state at room temperature (Figure 1).[19] The E–Z isomerization occurs by exposing the azobenzene derivatives to UV-irradiation, while the Z–E reverse isomerization occurs by thermal relaxation.[20]

Introducing azobenzene to polymer chains gained scientists' attention because azobenzene correlates with the polymer chains, which leads to a change in the mechanical response to light.[21] This work investigates the photoswitching kinetics of the polyelectrolyte brush films of polyacrylic acid (PAA) doped with methyl orange (MO) from E-state to Z-state by UV-light irradiation, and back reverse thermal relaxation to E-state . The time evolution of the photoisomerization and reverse thermal relaxation isomerization was studied using a novel model to understand the variation of the absorbance spectra and the electrical conductivity of the PAA-MO PEBs film. In addition, the chemical and morphological properties for the E- and Z-state of the PAA-MO PEBs film was studied.

2 | EXPERIMENTAL DETAILS

Polyacrylic acid (PAA, $[C_3H_4O_2]_n$; M_w = 1800 g/mol), methyl orange (MO, $C_{14}H_{14}N_3NaO_3S$; M_w = 327.33 g/mol), and sodium hydroxide (NaOH; M_w = 40.00 g/mol) were purchased from Sigma-Aldrich. An amount of 1 g PAA

powder was dissolved in 100 mL water using a continuous stirrer at 80°C for 4 h. afterward, the sample was sonicated for 2 h at 80°C and then 0.1 g of MO powder was added under stirring for 2 h at room temperature (RT). A Stock solution of NaOH was prepared with distilled water (DW) in 0.2 M solution for calibrating the acidity (pH) of PAA-MO/water solution. Finally, the pH of the PAA-MO/water solution was calibrated to 7. PAA-MO film was deposited on a glass substrate using casting technique by "grafting-to" method by non-covalent interactions[22]. The film was dried from the solvent at 40°C in vacuum oven under full atmospheric pressure of nitrogen overnight, the film thickness deduced from the cross-sectional SEM micrograph was about 250 nm.

PAA-MO PEBs film was irradiated by a UV-light (area: 432 × 356 mm) source with 366 nm wavelength and 15 W of power (<100 μW/mm²) for 0, 1, 2, 3, and 4 minutes. The absorbance spectra, the electrical conductivity, and the conductivity mapping were measured versus UV-irradiation exposure time using UV–Vis spectrophotometer (U-3900H) and 4-point probe (Microworld Inc.) equipped with a high-resolution multimeter (Keithley 2450 Sourcemeter). UV-irradiation was used to transfer the system from E-state to Z-state while the reversible process transformation from Z-state to E-state was performed by thermal relaxation process at 343, 333, 323, and 313 K for exposure time of 0, 1, 2, 3, and 4 minutes. The chemical and morphological structure of PAA-MO PEBs film was characterized using Fourier transform infrared spectroscopy (FTIR) (Bruker Tensor 27 spectrometer) and Atomic force microscope (AFM) (SPM SmartSPM™-1000).

3 | RESULTS AND DISCUSSION

3.1 | Absorbance spectral analysis

The Figure 2a shows the absorbance spectra of the PAA-MO PEBs film exposed to UV-irradiation for different times. The absorbance spectra PAA-MO PEBs film before being exposed to the UV-irradiation (black line) exhibits two bands at 352 nm and 420 nm represents $S_1(n\pi^*)$ transition, and $S_2(\pi\pi^*)$ transition, respectively.[23] The magnitude of the two absorbance peaks were decreased after being irradiated with UV-light, determining the Z–E transformation. Moreover, the Z–E transformation of PAA-MO leads to a shift toward the red region. The shifts in $S_1(n\pi^*)$ transition band were more pronounced compared to the shift happening in the $S_2(\pi\pi^*)$ transition band (Figure 2b). There are no changes in the absorbance spectra after 4 minutes of UV-irradiation, emphasizing that a quasi-state of the photostationary phase occurs between E- and Z-states.[24]
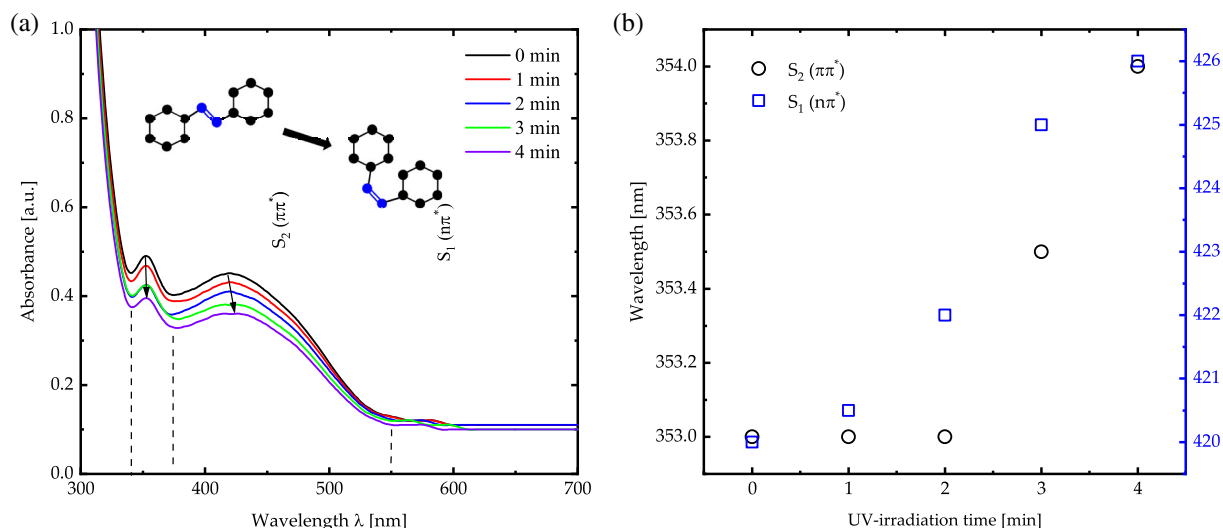
FIGURE 2 (a) Absorbance spectra and (b) the wavelength shifts of PAA-MO PEBs film after UV-irradiation of 0, 1, 2, 3, and 4 minutes. [Color figure can be viewed at wileyonlinelibrary.com]
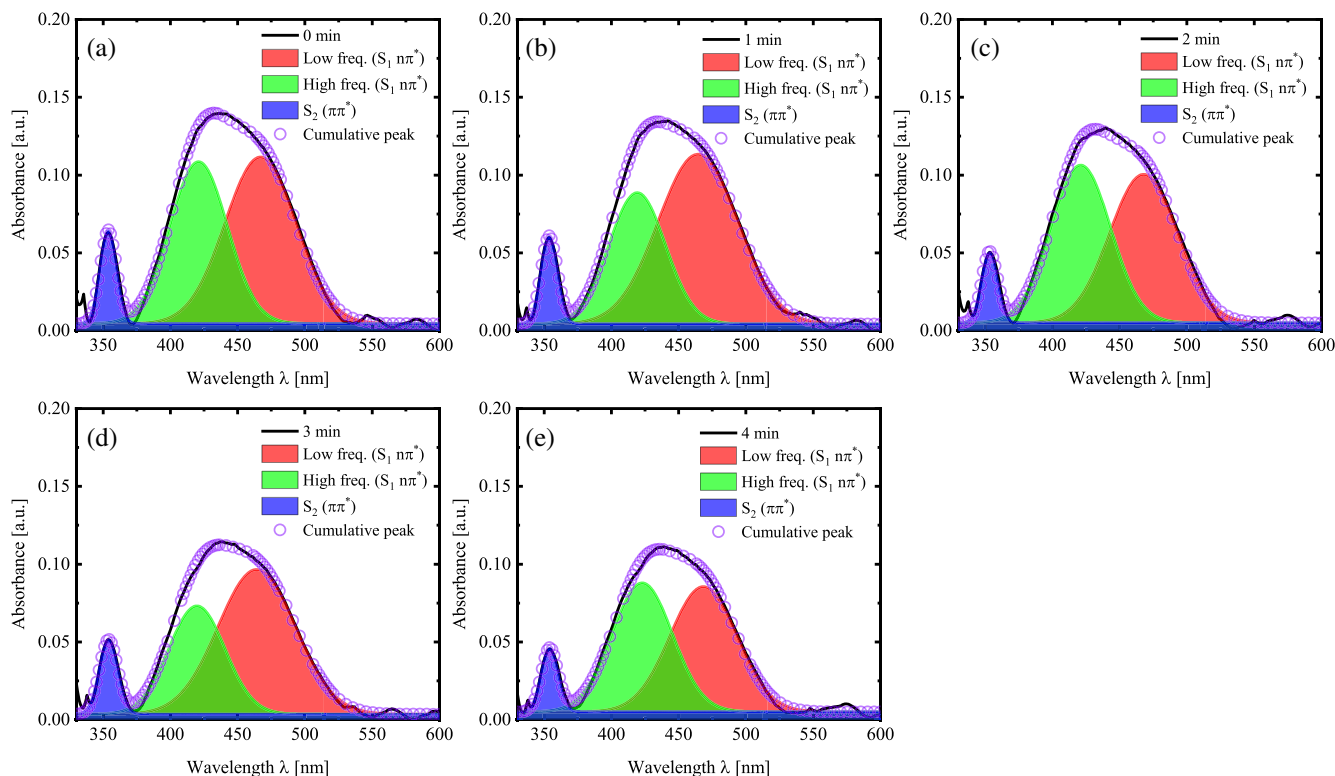

FIGURE 3 The de-convoluted of the absorbance band by fitting the spectra to three Gaussian peaks of the PEO-MO PEBs film by UV-irradiation times of 0, 1, 2, 3 and 4 minutes. [Color figure can be viewed at wileyonlinelibrary.com]

The $S_1(n\pi^*)$ transition band shows more than a single frequency band; since, the absorbance maxima do not decrease simply with increasing UV-irradiation time (Figure 2a). If the $S_1(n\pi^*)$ transition band was a single band, then the UV-irradiation should decrease the amplitude and increase the linewidth of the band.

Therefore, the $S_1(n\pi^*)$ transition bands upon UV-irradiation were most properly de-convoluted by fitting the absorbance envelope for two frequency bands. The spectral analysis of the $S_2(\pi\pi^*)$ transition, low- and high-frequency sides of the $S_1(n\pi^*)$ transition bands of the PAA-MO PEBs film upon UV-irradiation are shown in

Figure 3. The S1 absorbance band was de-convoluted by fitting the spectral envelope to three Gaussian peaks. The fitting converged with R^2 of about 0.99. De-convoluted
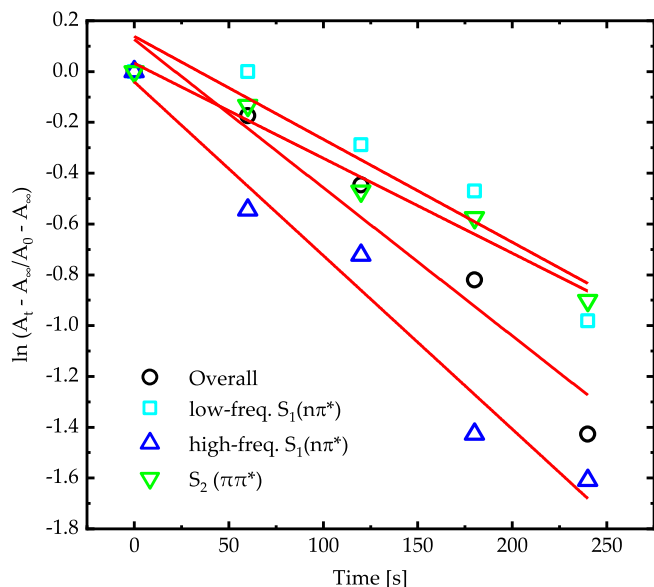

FIGURE 4 The kinetic constants for E–Z photoisomerization for overall absorbance peaks, low-frequency band of the $S_1(n\pi^*)$, high-frequency band of the $S_1(n\pi^*)$, and $S_2(\pi\pi^*)$ band. [Color figure can be viewed at wileyonlinelibrary.com]

was tested by fitting the absorbance band to Lorentzian, bi-Gaussian, and Voigt functions, but the fitting converge was poorer compared to the fitting to Gaussian function. Before fitting, the baseline was corrected according to the algorithm described in Reference 25.

The absorbance peaks exhibit three bands; $S_2(\pi\pi^*)$ transition, high- and low-frequency sides of the $S_1(n\pi^*)$ transition bands with maxima of 354 nm, 421 nm, and 467 nm, with linewidths of 14 nm, 50 nm, and 62 nm, respectively. The change in the overall absorbance peak with the UV-irradiation times was deduced from the superposition of the three Gaussian functions. Moreover, the three frequency bands experienced a red-shift (bathochromic) upon UV-irradiation. This indicates that MO is playing a gradual role of an H-bond donor, and consequently decreasing the energy bands in the $S_2(\pi\pi^*) \leftarrow S_0$ and $S_1(n\pi^*) \leftarrow S_0$ transitions.[26] Moreover, the continuous bathochromic shifts of the low-frequency band of the $S_1(n\pi^*)$ transition confirms the presence of the two distinct equilibria at configurations of hydrogen-bonding networks along between MO and PAA during the photoisomerization.[27]

The photoisomerization kinetics of the overall peak for PAA-MO PEBs film is the superposition of the photoisomerization kinetics of $S_2(\pi\pi^*)$ transition, low- and high-frequency sides of the $S_1(n\pi^*)$ transition bands, so
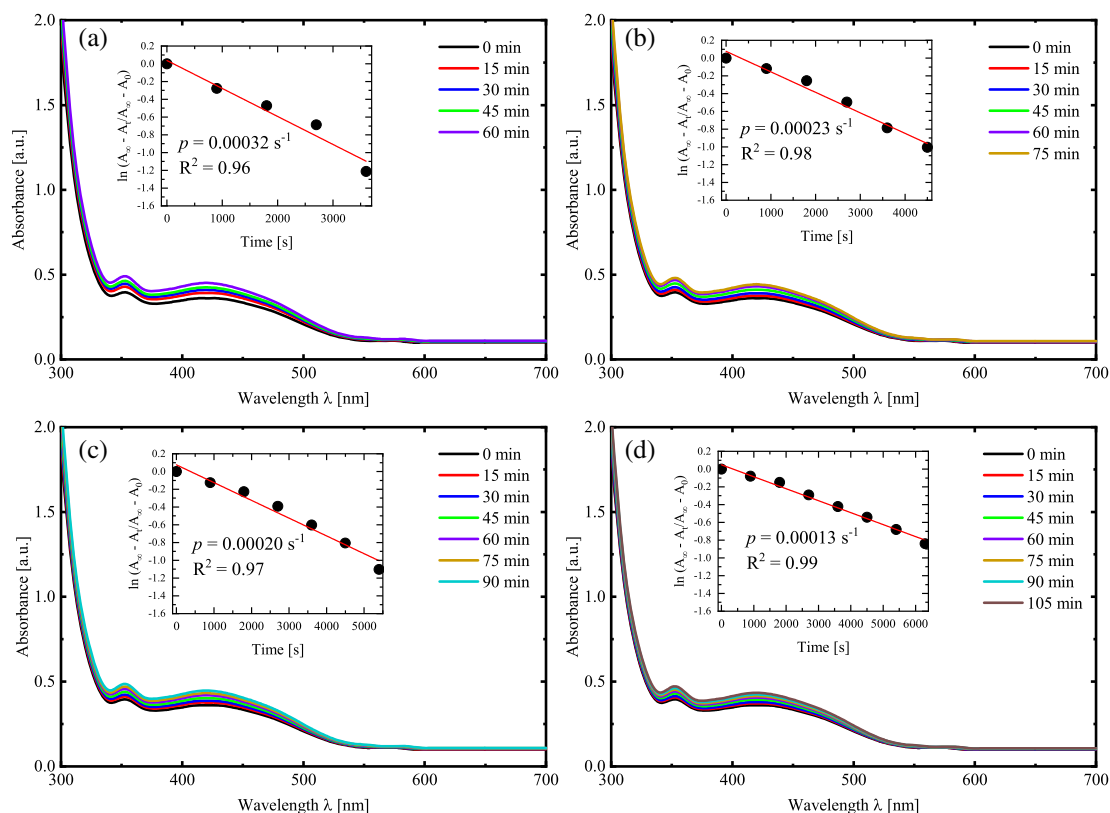

FIGURE 5 Time evolution for absorbance spectra of Z-state of PAA-MO PEBs film at temperatures (a) 343 K, (b) 333 K, (c) 323 K, and (d) 313 K. [Color figure can be viewed at wileyonlinelibrary.com]

the photoisomerization process is a combination of inter-molecular and dipole–dipole interactions. The first-order kinetics was used to calculate the photoisomerization rate constant (p), according to $\ln(A_t - A_\infty / A_0 - A_\infty) = -pt$, where: A_t, is the absorbance at each UV-irradiation time, A_∞ is the long UV-irradiation time, and A_0 is the initial state (E-state). Plotting the values of $\ln(A_t - A_\infty / A_0 - A_\infty)$ of overall absorbance peak, $S_2(\pi\pi^*)$ transition, low- and high-frequency sides of the $S_1(n\pi^*)$ transition bands for PAA-MO PEBs film versus the UV-irradiation time (t) yields the photoisomerization rate constant (p) by fitting the linear relation (Figure 4). The value of p for the overall peak was $0.0058\,\mathrm{s}^{-1}$, while the p value for $S_2(\pi\pi^*)$ transition, low- and high-frequency sides of the $S_1(n\pi^*)$ transition bands were 0.0037, 0.0041, and $0.0068\,\mathrm{s}^{-1}$, respectively. These results confirm that the photoisomerization kinetics of the overall peak for PAA-MO PEBs film is the superposition of the photo-isomerization kinetics of $S_2(\pi\pi^*)$ transition, low- and high-frequency of the $S_1(n\pi^*)$ transition bands. More-over, the time needed to transfer half E-state to Z-state is given by $\tau_{1/2} = \ln 2/p$. The $\tau_{1/2}$ of the photoisomerization of the PAA-MO PEBs is 1.99 minutes.
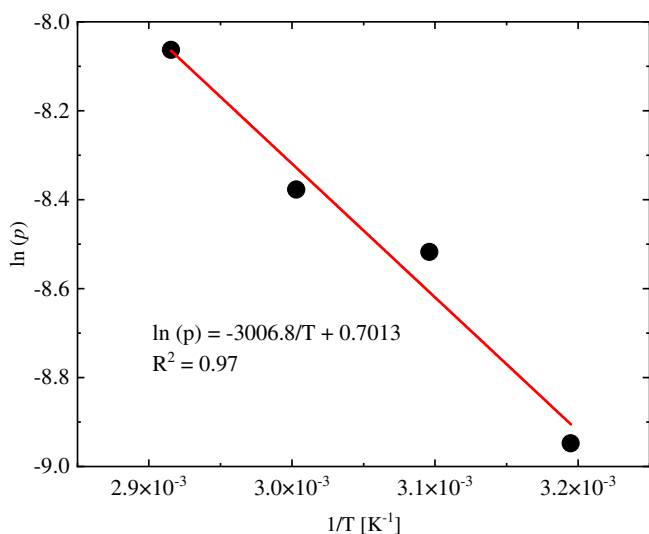
Figure 5 shows the absorbance spectra for the Z-state of PAA-MO PEBs film at temperatures of 343, 333, 323, and 313 K and for different thermal relaxation times. The magnitudes of $S_2(\pi\pi^*)$ and $S_1(n\pi^*)$ transition bands were increased with increasing the thermal relaxation time and they experienced a blue-shift, which means batho-chromic changes occur, consequently transforming more Z-states to E-states continuously. The reverse thermal isomerization rate can be calculated by plotting the values of $\ln(A_\infty - A_t / A_\infty - A_0)$ versus the thermal pro-cess time through fitting the linear relation (the inset of Figure 5). The values of p for the reverse isomerization at 343, 333, 323, and 313 K are 0.0032, 0.0023, 0.0020, and $0.0013\,\mathrm{s}^{-1}$, respectively. It can be concluded that increas-ing the temperature of the thermal relaxation leads to an increase in the reverse isomerization rate. The activa-tion energy (E_a) of the thermal isomerization and the Arrhenius constant (A) can be calculated using the Arrhenius equation $p = A\exp(-E_a/RT)$, where: R is the gas constant. Deduced activation energies value and the Arrhenius constants are presented in (Figure 6 and Table 1). Using the transition state theory, the standard enthalpy of activation $\Delta^\ddagger H^0$, the standard entropy of acti-vation $\Delta^\ddagger S^0$, the Gibbs free energy of activation $\Delta^\ddagger G^0$, and the quasi-equilibrium constant K are calculated using the following equations (Table 1)[24]:

$$E_a = \Delta^\ddagger H^0 + RT, \tag{1}$$

$$A = \frac{kTe}{h}\exp\left(\frac{\Delta^\ddagger S^0}{R}\right), \tag{2}$$

$$\Delta^\ddagger G^0 = \Delta^\ddagger H^0 - T\Delta^\ddagger S^0, \tag{3}$$

$$\Delta^\ddagger G^0 = -RT\ln K, \tag{4}$$

where: e is the Euler number (2.718).

3.2 | Electrical conductivity

According to the H. Rau study,[28] the E–Z transformation increased the dipole moment from 0.0 to 3.0 D. Conse-quently, the conductivity values increased with E–Z

FIGURE 6 Arrhenius plot of the isomerization relaxation of PAA-MO PEBs film from E- to Z-state after being transformed from Z- to E-state by UV-irradiation. [Color figure can be viewed at wileyonlinelibrary.com]

ln (p) = -3006.8/T + 0.7013
R^2 = 0.97

TABLE 1 The deduced thermodynamic parameters of the PAA-MO PEBs film which was exposed to reverse thermal transformation from E- to Z-state after the first transformation by UV-irradiation from Z- to E-state.

Isomerization energy E_a (10^4 J/m)	Arrhenius constant, $\ln(A)$	Enthalpy of isomerization $\Delta^\ddagger H^0$ (10^4 J/mol)	Entropy of isomerization $\Delta^\ddagger S^0$ (J/mol)	Gibbs free energy $\Delta^\ddagger G^0$ (10^3 J/mol)	Equilibrium constant K
2.499	0.701	2.227	−16.329	5.358	0.140

transformation. Figure 7 shows the average conductivity values for the PAA-MO PEBs film as a function of UV-irradiation times. It can be seen that the average conductivity increased with increasing the UV-irradiation time.
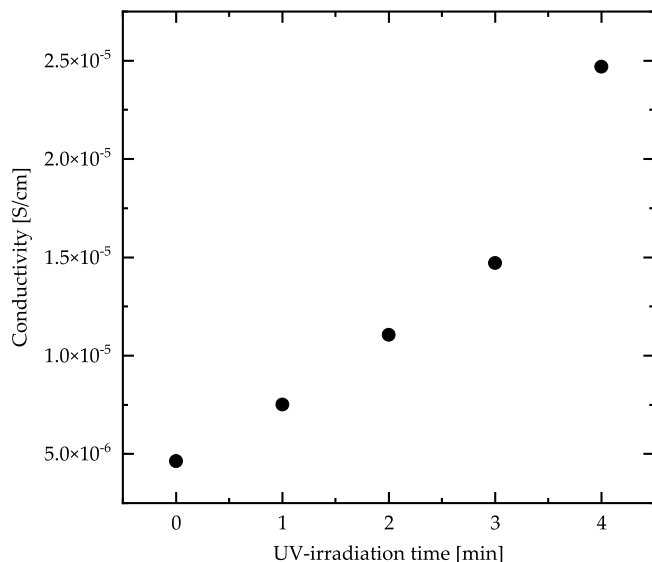

FIGURE 7 The electrical conductivity of PAA-MO PEBs film as a function of UV-irradiation time

The conductivity mapping (1 cm × 1 cm) of PAA-MO PEBs film at the initial state (*E*-state) (Figure 8a) shows the significant variation of the conductivity across the film due to the distribution and concentration of the *E*-state to *Z*-state, the variation of the growth process of the film, and the quality of the transfer process. Applied UV-irradiation on the PAA-MO PEBs film leads to increased *Z*-state continuously compared to *E*-state, which means an increase in the conductivity across the film (Figure 8b–e).

3.3 | Chemical and morphological properties

The chemical structure of the PAA-MO PEBs film in the *E*- and *Z*-states was studied using FTIR spectra (Figure 9). The absorption band at 1100 cm^{-1} attributed to the stretching C—O bonds in the PAA, and the absorption peak at 1554 cm^{-1} represents the symmetric COO$^-$ of carboxylate in PAA. The CH$_x$ and OH bonds in the PAA appeared at 2929 cm^{-1} and 3200 cm^{-1}, respectively.[29] Moreover, the S=O vibrational band in MO is at 1150 cm^{-1}, while C—N stretching vibrational band in MO
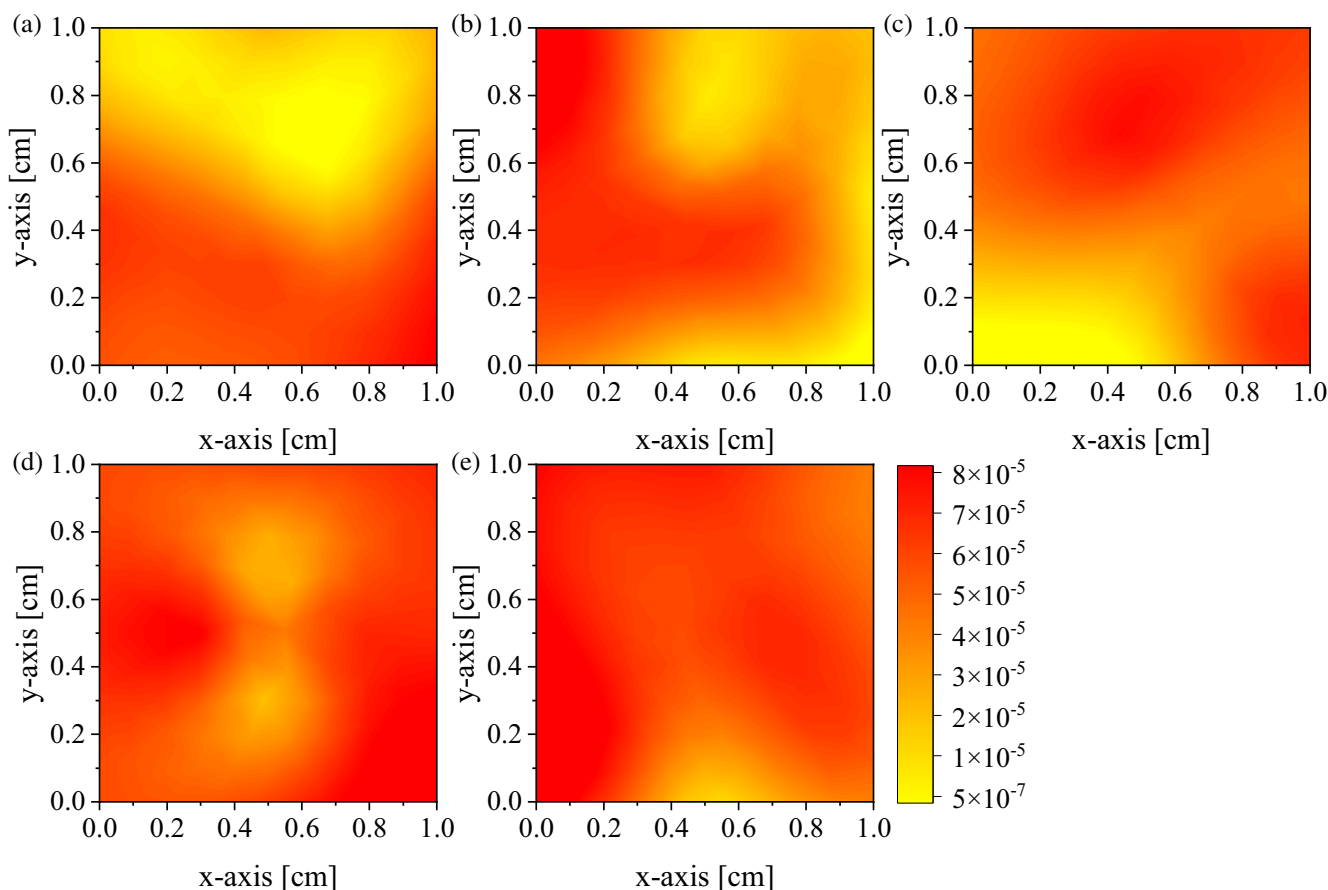

FIGURE 8 The 2D electrical conductivity maps acquired on area (1 cm × 1 cm) of PAA-MO PEBs film at (a) initial state (*E*-state), and after (b) 1, (c) 2, (d) 3, and (e) 4 minutes of UV-irradiationtimes. [Color figure can be viewed at wileyonlinelibrary.com]

is at $1340\,cm^{-1}$. The absorption band at $1390\,cm^{-1}$ is assigned to N=N vibrational band in MO. Finally, the N—H stretching vibrational band is at $3360\,cm^{-1}$.[30] The FTIR spectra of E- and Z-states of the PAA-MO PEBs films show identical vibrational bands with a little shift in the N=N vibrational band, which indicates the Z–E transformation around N=N bands.[24]

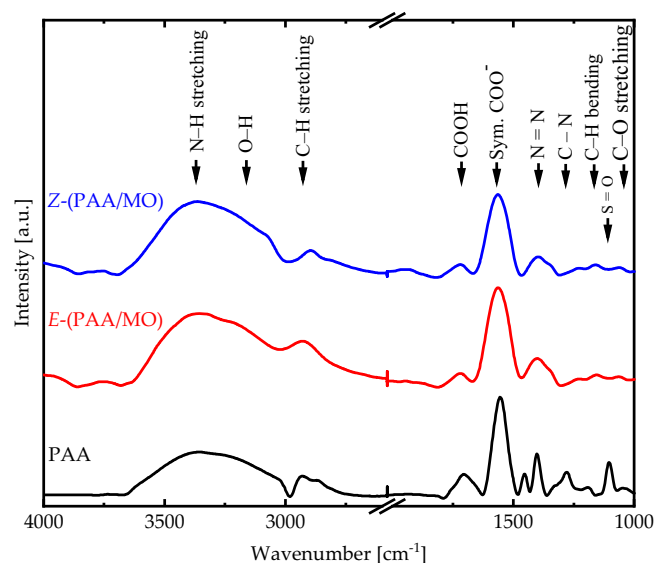The morphological properties of the PAA-MO PEBs film at E- and Z-states were investigated using AFM measurements (Figure 10). At pH equal to 7, the COOH for pure PAA PEBs film transform to COO^- groups, this leads to create swollen brushes (Figure 10a). The film in E-state shows a stretching brush-like structure distributed randomly in seperated islands (Figure 10b). Moreover, transforming the film from E- to Z-state was led the brush to collapse due to the angular rotational momentum upon E–Z isomerization (Figure 10c).[31] Finally, the roughness in the E-state was decreased from 3 nm to 2 nm when transforming from E- to Z-state.

FIGURE 9 FTIR spectra of PAA film and PAA-MO PEBs film at E- and Z-states. [Color figure can be viewed at wileyonlinelibrary.com]

4 | CONCLUSIONS

The absorbance band peaks exhibit three bands; $S_2(\pi\pi^*)$ transition, high- and low-frequency sides of the $S_1(n\pi^*)$ transition bands. The results confirm that the photoisomerization kinetics of the overall peak of PAA-MO PEBs film is the superposition of the photoisomerization kinetics of $S_2(\pi\pi^*)$ transition, low- and high-frequency of the $S_1(n\pi^*)$ transition bands. The MO is playing a gradual role of an H-bond donor, and consequently decreasing the energy bands in the $S_2(\pi\pi^*) \leftarrow S_0$ and $S_1(n\pi^*) \leftarrow S_0$ transitions. The 2D electrical conductivity maps at E-state shows the significant variation across the film. The electrical conductivity increased after UV-irradiation which is associated to the increase in the Z-state due to the transformation from E- to Z-state. The transformation from E-to Z-state was led to collaps the brush-like structure because of the angular rotational momentum upon E–Z isomerization.
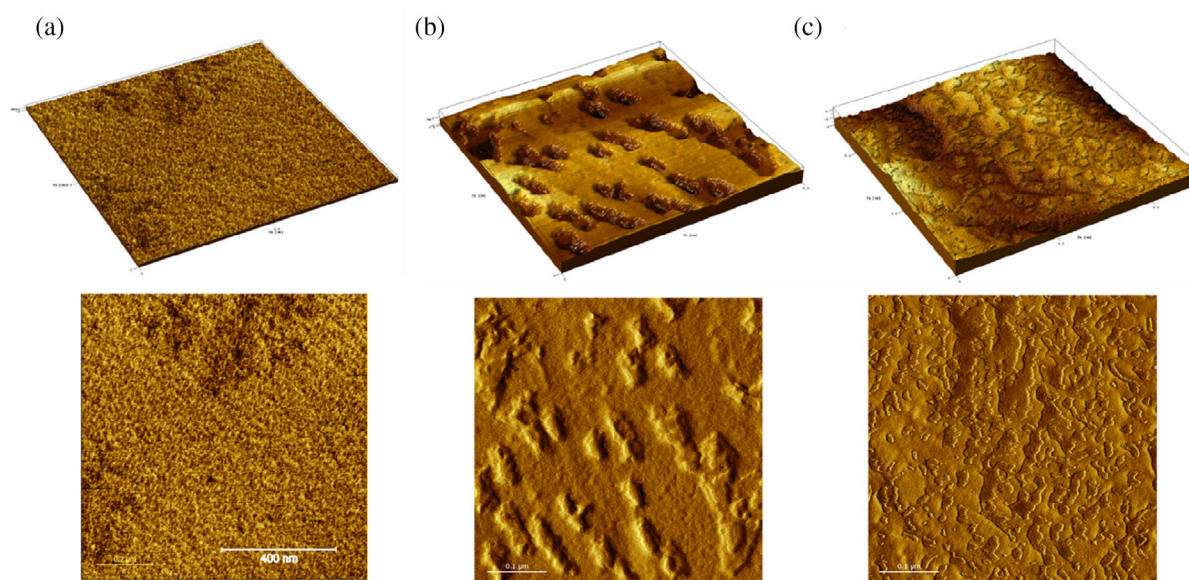

FIGURE 10 3D and 2D AFM images of (a) pure PAA, and PAA-MO PEBs film at (b) E-state and (c) Z-state. [Color figure can be viewed at wileyonlinelibrary.com]

AUTHOR CONTRIBUTIONS

Qais M. Al-Bataineh: Conceptualization (lead); visualization (lead); writing – original draft (equal). **Ahmad A. Ahmad:** Formal analysis (equal); resources (lead); writing – review and editing (equal). **Areen A. Bani-Salameh:** Formal analysis (equal); investigation (equal); methodology (supporting). **Rund Abu-Zurayk:** Investigation (equal); validation (equal); writing – review and editing (equal). **Roland Hergenröder:** Data curation (equal); supervision (lead); writing – review and editing (equal). **Ahmad D. Telfah:** Formal analysis (equal); visualization (supporting); writing – original draft (equal).

ACKNOWLEDGMENTS

CONFLICT OF INTEREST

The authors declare no potential conflict of interest.

DATA AVAILABILITY STATEMENT

Data sharing is not applicable to this article as no new data were created or analyzed in this study.

ORCID

Qais M. Al-Bataineh https://orcid.org/0000-0003-2852-4781

Ahmad D. Telfah https://orcid.org/0000-0003-1478-8620

Ahmad A. Ahmad https://orcid.org/0000-0001-7488-7781

REFERENCES

[1] J. Yuan, H. S. Antila, E. Luijten, *Macromolecules* **2020**, *53*, 2983.

[2] S. Das, M. Banik, G. Chen, S. Sinha, R. Mukherjee, *Soft Matter* **2015**, *11*, 8550.

[3] G. Ferrand-Drake del Castillo, R. L. Hailes, A. Dahlin, *J. Phys. Chem. Lett.* **2020**, *11*, 5212.

[4] J. Yuan, H. S. Antila, E. Luijten, *ACS Macro Lett.* **2019**, *8*, 183.

[5] W. Guo, H. Xia, F. Xia, X. Hou, L. Cao, L. Wang, J. Xue, G. Zhang, Y. Song, D. Zhu, *ChemPhysChem* **2010**, *11*, 859.

[6] Q. Cao, C. Zuo, L. Li, Y. Zhang, G. Yan, *J. Polym. Sci., Part B: Polym. Phys.* **2012**, *50*, 805.

[7] D. Aulich, O. Hoy, I. Luzinov, M. Brücher, R. Hergenröder, E. Bittrich, K.-J. Eichhorn, P. Uhlmann, M. Stamm, N. Esser, *Langmuir* **2010**, *26*, 12926.

[8] Y. S. Park, Y. Ito, Y. Imanishi, *Macromolecules* **1998**, *31*, 2606.

[9] E. Currie, A. Sieval, G. Fleer, M. C. Stuart, *Langmuir* **2000**, *16*, 8324.

[10] Z.-Y. Zhang, Y. He, Z. Wang, J. Xu, M. Xie, P. Tao, D. Ji, K. Moth-Poulsen, T. Li, *J. Am. Chem. Soc.* **2020**, *142*, 12256.

[11] D. Mulatihan, T. Guo, Y. Zhao, *Photochem. Photobiol.* **2020**, *96*, 1163.

[12] A. N. Zaid, M. Hassan, N. Jaradat, M. Assali, R. Al-Abbassi, A. Alkilany, S. R. Abulateefeh, *Mater. Res. Exp.* **2020**, *6*, 1250d7.

[13] X. Fu, J. Yu, N. Dai, Y. Huang, F. Lv, L. Liu, S. Wang, *ACS Appl. Bio Mater.* **2020**, *3*, 4751.

[14] H. Liu, Y. Feng, W. Feng, *Compos. Commun.* **2020**, *21*, 100402.

[15] H. Liu, B. Xu, X. Yang, Z. Li, Z. Mo, Y. Yao, S. Lin, *Compos. Commun.* **2020**, *19*, 233.

[16] E. Fuentes, M. Gerth, J. A. Berrocal, C. Matera, P. Gorostiza, I. K. Voets, S. Pujals, L. Albertazzi, *J. Am. Chem. Soc.* **2020**, *142*, 10069.

[17] H. Hongchao, C. Yingde, *Synth. Met.* **2015**, *205*, 106.

[18] D. Bléger, J. Dokic, M. V. Peters, L. Grubert, P. Saalfrank, S. Hecht, *J. Phys. Chem. B* **2011**, *115*, 9930.

[19] Q. M. Al-Bataineh, A. A. Ahmad, A. M. Alsaad, A. Telfah, *Polymer* **2020**, *12*, 2954.

[20] Q. M. Al-Bataineh, A. Ahmad, A. Alsaad, I. Qattan, A. A. Bani-Salameh, A. D. Telfah, *Polymer* **2020**, *12*, 1275.

[21] M. Liu, L. Yin, L. Wang, T. Miao, X. Cheng, Y. Wang, W. Zhang, X. Zhu, *Polym. Chem.* **2019**, *10*, 1806.

[22] S. Ma, X. Zhang, B. Yu, F. Zhou, *NPG Asia Mater.* **2019**, *11*, 1.

[23] J. N. Bull, M. S. Scholz, E. Carrascosa, E. J. Bieske, *Phys. Chem. Chem. Phys.* **2018**, *20*, 509.

[24] A. A. Ahmad, Q. M. Al-Bataineh, A. M. Alsaad, D. M. Al-Nawafleh, A. M. Al-Nawafleh, A. D. Telfah, *Photochem. Photobiol.* **2021**, *98*, 823.

[25] K. H. Liland, T. Almøy, B.-H. Mevik, *Appl. Spectrosc.* **2010**, *64*, 1007.

[26] Y. Al-Abdallat, I. Jum'h, A. Al Bsoul, R. Jumah, A. Telfah, *Water, Air, Soil Pollut.* **2019**, *230*, 1.

[27] P. Ruzza, R. Hussain, B. Biondi, A. Calderan, I. Tessari, L. Bubacco, G. Siligardi, *Biomolecules* **2015**, *5*, 724.

[28] H. Rau, *Photochem. Photophys.* **1990**, *2*, 119.

[29] X. Yi, Z. Xu, Y. Liu, X. Guo, M. Ou, X. Xu, *RSC Adv.* **2017**, *7*, 6278.

[30] T. Shen, C. Jiang, C. Wang, J. Sun, X. Wang, X. Li, *RSC Adv.* **2015**, *5*, 58704.

[31] A. A. Ahmad, Q. M. Al-Bataineh, D. M. Al-Nawafleh, A. D. Telfah, *Photochem. Photobiol.* **2021**, *98*, 831.